Passive Stabilization in a Linear MHD Stability Code

A. M. M. Todd*

Plasma Physics Laboratory, Princeton University

Princeton, New Jersey 08544

ABSTRACT

Utilizing a Galerkin procedure to calculate the vacuum contribution to the ideal MHD Lagrangian, we describe the implementation of realistic boundary conditions in a linear stability code. The procedure permits calculation of the effect of arbitrary conducting structure on ideal MHD instabilities, as opposed to the prior use of an encircling shell. The passive stabilization of conducting coils on the tokamak vertical instability is calculated within the PEST code and gives excellent agreement with 2-D time dependent simulations of PDX.

Introduction

The structure and growth rates of ideal MHD instabilities are strongly dependent on the imposed boundary conditions. This is particularly true of the vertical instability in tokamaks, where flux compression against a perfectly conducting shell in the vacuum region can provide significant stabilization of the mode, even when the shell is far from the plasma. Lust and Martenson[1] have shown that expressing the perturbed vacuum magnetic field in terms of the gradient of a single-valued scalar potential alone, cannot describe this effect. In addition, Jardin[2] has shown that flux compression against coils embedded in the vacuum results in induced currents whose effect on the stability of this mode is critically dependent on the external circuitry of the coil system.

For nonaxisymmetric modes, existing linear stability codes such as PEST[3] can only surround a plasma with an encircling wall in the vacuum on which the normal component of the perturbation is zero. In practice, the conducting structure in a tokamak may be more irregular and topologically complicated, as in a double-null divertor configuration.

Since time-dependent MHD calculations are comparatively expensive, it is desirable to include such effects in a linear stability code. Dewar[4] has recently reformulated the energy principle in a manner which makes the inclusion of the appropriate boundary conditions straight-forward. In the following sections we describe the formulation and numerical implementation of this procedure for calculating the vacuum energy, various verifications

that have been performed, and finally a comparison with 2-D time dependent simulations of PDX.

Formulation

Consider N conducting elements of arbitrary cross section that can carry induced toroidal currents, embedded in a vacuum region V and surrounded by an encircling wall that may be removed to infinity. As is shown in Fig. 1, the plasma is the N +1st conducting element, the wall is the N +2nd element with respect to induced poloidal currents, and unit normals $\hat{\underline{n}}$ point into V.

Dewar[4] has shown that the vacuum energy contribution to the Lagrangian for a perturbation $\vec{\xi}$ can be written as

$$\delta W_v = \frac{1}{2}\, \underline{i}^{*} \underset{\sim}{L} \underline{i} + \frac{\mu_o}{2} \int_V \nabla\chi^{*} \cdot \nabla\chi \, d\tau \quad , \tag{1}$$

where χ is the usual scalar potential for the perturbed vacuum field; $\underset{\sim}{L}$ is the inductance matrix, and i is the vector of perturbed currents $i_1, i_2, \ldots i_{n+2}$ induced in the $N + 2$ conductors.[a] The first term in Eq. (1) is the stored energy in the conductors. The currents are defined by Faraday's law

$$\frac{d}{dt} (\underset{\sim}{L} \underline{i} - \underline{e}) = \underline{0} \tag{2}$$

(a) We will use complex expansion functions rather than sine and cosine components; hence the use of * to denote the complex conjugate transpose, despite the fact that many quantities such as $\underline{i}$ are real.

where $\underline{e}$ is the vector of induced fluxes linking the circuits.

The high frequency inductance matrix is defined by

$$\underset{\sim}{L} = \int_V \vec{\underline{Y}} \cdot \vec{\underline{Y}}^* \, d\tau \quad , \tag{3}$$

where $\vec{\underline{Y}}(\vec{\underline{Y}}^*)$ is the one-dimensional column (row) matrix of magnetic intensities generated by unit currents in the N + 2 elements, that satisfies

$$\hat{n} \cdot \vec{\underline{Y}} = \underline{0} \qquad \text{on} \qquad S_\ell ; \; \ell = 1, \; 2 \ldots N + 2 \; . \tag{4}$$

Our Galerkin procedure expands the scalar potential

$$\chi = \underline{u}^* \underline{\nu} \tag{5}$$

in terms of functions $\underline{u}$ that satisfy Laplace's equation in V, and hence Maxwell's equations for the perturbed field $\nabla\chi$. By extremizing the perturbed field energy in the vacuum with respect to $\underline{\nu}^*$, we obtain the coefficients $\underline{\nu}$ from

$$\underset{\sim}{A}\underline{\nu} = \frac{1}{\mu_o} \int_{S_{N+1}} \hat{n} \cdot \vec{\xi} (\vec{B} \cdot \nabla) \underline{u} \, dS \; , \tag{6}$$

where $\vec{B}$ is the unperturbed magnetic field, and

$$\underset{\sim}{A} = - \sum_{\ell=1}^{N+2} \int_{S_\ell} u (\hat{n} \cdot \nabla) u^* \, dS \; . \tag{7}$$

A similar expansion for

$$\vec{\underline{Y}} = \vec{\underline{K}} + \nabla(\underset{\sim}{\lambda}^{*}\underline{u}) \tag{8}$$

in terms of the same functions u as are used for axisymmetric modes, must also satisfy Maxwell's equations in V, the additional vector $\vec{\underline{K}}$ being introduced for the unit current requirement

$$\oint_{C_\ell} \vec{Y}_k \cdot \vec{d\ell} = \delta_{k\ell} \qquad k, \ell = 1, 2 \ldots N+2 \ . \tag{9}$$

In this case, extremizing the induced energy in the conductors with respect to $\underset{\sim}{\lambda}^{*}$ yields the coefficient matrix

$$\underset{\sim}{\lambda} = \underset{\sim}{A}^{-1}\underset{\sim}{C} \ , \tag{10}$$

where

$$\underset{\sim}{C} = \sum_{\ell=1}^{N+2} \int_{S_\ell} \underline{u}(\hat{n}\cdot\vec{\underline{K}}^{*}) \, dS \ . \tag{11}$$

This has been shown[4] to correspond to satisfying the boundary conditions of Eq. (4) for $\vec{\underline{Y}}$. In a (ψ, θ, ϕ) flux coordinate system of Jacobian J, we decompose the perturbation into a finite number of poloidal harmonics M, and from axisymmetry a single toroidal harmonic n,

$$\vec{\xi}\cdot\vec{dS} = \sum_{m=1}^{M} \xi_m \exp[i(m\theta - n\theta)]J \, d\theta d\phi \ , \tag{12}$$

and introduce the integrals

$$\underline{\Lambda}(m) = \int_{S_{N+1}} \exp[i(m\theta - n\phi)](\vec{B}\cdot\nabla)\underline{u}J \, d\theta d\phi \quad , \tag{13}$$

$$\underline{\Omega}(m) = \int_{S_{N+1}} \exp[i(m\theta - n\phi)](\vec{B}\cdot\vec{K}) J \, d\theta d\phi \quad . \tag{14}$$

Then using Green's theorem and the Hermitian nature of $\underset{\sim}{A}$, together with Eqs. (6) and (13), we can express the perturbed vacuum field energy

$$\frac{\mu_o}{2} \int \nabla\chi^*\cdot\nabla\chi \, d\tau = \frac{1}{2\mu_o} \sum_{m,m'=1}^{M} \xi^*_{m'} \, \underline{\Lambda}^*(m')\underset{\sim}{A}^{-1}\underline{\Lambda}(m)\xi_m \quad . \tag{15}$$

In order to calculate the induced currents, we utilize the fact that in our linear problem, the currents and fluxes are in phase with the perturbation. We can then write Eq. (2) as

$$\underset{\sim}{L}\underline{i} - \int_{S_{N+1}} \hat{n}\cdot\vec{\xi}(\vec{B}\cdot\underline{Y}) \, dS = \underline{e} \quad , \tag{16}$$

where the second term results from the time rate of change of inductance due to the perturbation. However, before we can solve this equation, we must apply Kirchhoff's laws to the external

circuitry linking the N + 2 conductors and construct constraints for the currents and fluxes in some form

$$\underset{\sim}{P}\underline{i} + \underset{\sim}{Q}\underline{e} = \underline{0} \ . \tag{17}$$

Now combining Eqs. (16) and (17) yields

$$\underset{\sim}{D}\underline{J} = \underline{F} \ , \tag{18}$$

where

$$\underset{\sim}{D} = \begin{pmatrix} \underset{\sim}{L} & -\underset{\sim}{I} \\ \underset{\sim}{P} & \underset{\sim}{Q} \end{pmatrix} \ , \tag{19}$$

$$\underline{J} = \begin{pmatrix} \underline{i} \\ \underline{e} \end{pmatrix} \ , \tag{20}$$

$$\underline{F} = \begin{pmatrix} \sum_{m=1}^{M} \xi_m \underline{T}(m) \\ \underline{0} \end{pmatrix} \ , \tag{21}$$

$\underset{\sim}{I}$ is the unit matrix, and

$$\underline{T}(m) = \underline{\Omega}(m) + \underset{\sim}{\lambda}^{*}\underline{\Lambda}(m) \ . \tag{22}$$

Then the stored energy

$$\frac{1}{2}\,\underline{i}^{*}\underset{\sim}{L}\underline{i} = \frac{1}{2}\,J^{*}\,\underset{\sim}{D}\underline{J} = \frac{1}{2}\sum_{m,m'=1}^{M} \xi_{m'}^{*}\,\underline{T}^{*}(m')\underset{\sim}{D}^{-1}\underline{T}(m)\,\xi_m \ , \tag{23}$$

2. Radiative Processes in the Soft X-ray Regime

A fairly complete description of the x-ray emission from hydrogen ions and impurities in the plasma may be found elsewhere in the literature.[1] Here we summarize conclusions of that discussion.

We first consider bremsstrahlung. For a Maxwellian plasma the power dW emitted per photon energy interval dk by bremsstrahlung is given by

$$\left(\frac{dW}{dk}\right)_{brems.} = 3 \times 10^{11} \frac{n_e \Sigma n_i Z_i^2}{10^{26} cm^{-3}} \left(\frac{T_e}{keV}\right)^{-1/2} \bar{g}_{ff}(T_e, k) \exp(-k/T_e) \, sec^{-1}$$

where n_e and n_p are the electron and ion densities, respectively, T_e the electron temperature, Z_i the positive ion charge, k the photon energy, and $\bar{g}_{ff}$ the temperature-averaged Gaunt factor, normally taken equal to unity. The electron temperature is then found as the inverse of the slope in a semilogarithmic plot of the intensity dW/dk vs. photon energy. Strictly speaking, this procedure is valid only when applied to the Abel inverted spectra. One may nonetheless obtain a good approximation to the electron temperature directly from the raw spectra if one considers only the high energy region of the continuum where so-called "profile effects"[1] are less important.

Next we consider x-ray radiation that results when free electrons recombine into unoccupied energy levels of impurity ions. Again, for a Maxwellian plasma with ion density n_i of charge $Z_i - 1$, ground state ionization potential χ_i, and principal quantum number n, the x-ray intensity is given by

satisfies Eq. (9) but also the boundary condition Eq. (4) exactly. For all other k = 1, 2,... N + 1, we choose $\vec{K}_k$ to be the poloidal field intensity generated by two sets of toroidal hoop current sources. The first set is located within C_k and sums to unity to satisfy Eq. (9); the locations being chosen so as to generate poloidal field lines that closely conform to the shape of C_k. Thus a circular coil is well represented by a single unit source at its center, whereas a thin conducting plate may require several sources (L) whose sum is unity, in a line along the midplane. The second set consists of image sources outside the wall whose function is to ensure that the normal component of the poloidal field at the wall is zero. In practice, we choose the positions and strengths of the first set, and the L' positions for the image sources. The required image source strengths for each k = 1,. . . N + 1 at these same L' positions are then calculated using the procedure described in Johnson et al.,[5] whereby an MHD equilibrium solution is forced to conform to a given plasma shape. Thus

$$\vec{K}_k(\vec{r}) = \sum_{j=1}^{L+L'} a_{kj} I_{kj} \nabla\phi \times \nabla G_{kj}(\vec{r}/\vec{r}_{kj}) \tag{26}$$

where G_{kj} is the Green's function for a toroidal hoop at radius a_{kj} carrying a current I_{kj}. The dominant contribution to the inductance matrix is thus provided by

$$Z_{kj} = \int_V \vec{K}_k \cdot \vec{K}_j^* \, d\tau = -\frac{1}{4\pi^2} \sum_{\ell=1}^{N+2} \int \nabla\phi^2 \sum_{p=1}^{L+L'} \sum_{q=1}^{L+L'} I_{kp} I_{jq} a_{kp} a_{jq} G_{kp} \frac{\partial G_{jq}}{\partial n} \, dS \,, \tag{27}$$

where the inductance matrix

$$\underset{\sim}{L} = \mu_o(\underset{\sim}{Z} - \underset{\sim}{C}^*\underset{\sim}{\lambda}) \ . \tag{28}$$

The second term in Eq. (28) is the correction supplied by the expansion functions $\underset{\sim}{u}$ to the boundary condition requirement of Eq. (4). These functions need only satisfy Laplace's Equation in V. We therefore, choose to expand in a toroidal harmonics[6]

$$u^n_{k+1} = (\cosh \mu - \cos \eta)^{1/2} \exp[i(n\phi + k\eta)] P^n_{k-1/2}(\mu) \ . \tag{29}$$

Here μ, η, ϕ are the toroidal coordinates based on some toroidal axis, $P^n_{k-1/2}$ are Legendre polynomials of order n and degree k $-1/2$. Several degrees of polynomials for the appropriate toroidal mode numbers n, centered at various axes are used. We choose one axis for each current source point (internal and image), except for the plasma sources k = N + 1. In this latter case, adequate modeling of ξ^* has been shown to require many axes on some flux surface within the plasma, spaced in equal increments of the poloidal angle θ. While it is not clear that this is the best choice, satisfactory results have been obtained.

Comparison tests with other methods for calculating δW_V[7] have shown that using three degrees of harmonics (k = -1, 1, 2) is optimal. Further, with a single current source at the magnetic axis and sixteen toroidal axes on a flux surface at approximately 0.8 of the minor radius to model the plasma, and eight image sources and harmonic axes to model the wall; agreement of δW_V to within 1% can be obtained for many plasma shapes and a wide range

of wall positions. The corresponding differences in growth rate as calculated with PEST, are of the same order. The addition of coils and other conducting members in V requires additional sources and harmonics, usually one per member unless the shape is complex. The vector of expansion functions $\underline{u}$ is then composed of all the degrees of harmonics at all the axes used in the problem.

Numerical Procedure

We adopt the convention of Jardin[2] to identify the conductor circuitry. From this convention, an algorithm identifies the Kirchhoff constraints and loads the $\underset{\sim}{P}$ and $\underset{\sim}{Q}$ matrices of Eq. (17) by equating the appropriate currents and fluxes for multiple turn coils. Positive turns imply connections where the induced current flows in the $\hat{\phi}$ direction.

Then, given the parameters of some plasma equilibrium configuration we construct the expansion function $\underline{\vec{K}}$ and $\underline{u}$, and evaluate the surface integrals $\underset{\sim}{Z}$, $\underset{\sim}{A}$, $\underset{\sim}{C}$, $\underline{\Lambda}$, $\underline{\Omega}$ in Eqs. (27), (7), (11), (13), and (14) respectively. Clearly only $\underset{\sim}{A}$ and $\underline{\Lambda}$ are relevant for $n \neq 0$. Equation (10) is solved for $\underset{\sim}{\lambda}$ to calculate the inductance matrix $\underset{\sim}{L}$ from Eq. (28) and hence the augmented matrix $\underset{\sim}{D}$. Finally, the vacuum energy is calculated from Eq. (24) and stored for the eigenmode analysis of PEST.

Code Testing

Using a single central source and three harmonics at the same axis, comparison of the high-frequency inductance of a torus was made with the analytic calculations of Malmberg and

Rosenbluth.[8] Except at aspect ratios which are less than 2.0, and hence rare for our purposes, the agreement is better than 1%. For an extremely tight torous of aspect ratio 1.2, the agreement is within 30%; this compares with the standard zero skin depth limit of the low-frequency value which is a factor of five higher. Equivalent analytic results for other shapes are scarce. However, comparisons with other zero skin depth limit low-frequency self and mutual inductances for square cross section tori and concentric toroidal shells show reasonable agreement at large aspect ratios, where the differences due to nonuniformity of the skin current should be small.

We next compared the Lust-Martenson corrections to cylindrical analytic results. Given a zero beta equilibrium solution for an elliptic plasma, the contributions to δW_V due to poloidal and toroidal flux compression against a confocal wall can be calculated analytically.[9] Numerical calculation of such equilibria, but at aspect ratio 100, and subsequent numerical evaluation of δW_V were found to agree for a variety of confocal walls to within 0.1%. The relative weight of the poloidal and toroidal contributions were widely varied in these tests suggesting accurate calculation of both components. The addition of other conducting elements in the vacuum is just a generalization of such a Lust-Martenson calculation.

Finally, to check that the perturbed field energy contribution is also handled correctly, comparisons have been made with other numerical methods.[7] We have previously alluded to such

calculations and show in Table I the excellent agreement with the current PEST vacuum calculation.

Finally, we have compared the results of the linear growth rate of the vertical instability for several PDX equilibria with the 2-D time-dependent code of Jardin.[2] Table II shows a comparsion of the growth rates for the case with no conductors, and with the two circuits shown in Fig. 2a. The importance of the external circuitry is clear. Additional calculations for this case show that flux compression results in stability for a wall one minor radius from the plasma, and for the two rectangular plates shown in Fig. 2b. Each linear stability run with all 14 coils requires less than 10 minutes on a CDC 7600, compared with approximately 30 minutes for the corresponding time-dependent calculation.

Conclusions

We have implemented a new method for calculating the vacuum contribution to the Lagrangian within PEST. Tests show we can now calculate the important effect of passive stabilization on the axisymmetric instability. In addition, we can treat the effect of realistic structure on all toroidal mode numbers.

Acknowledgments

The author is greatly indebted to Dr. R. L. Dewar whose help in this application of his procedure was invaluable. In addition, the work of Drs. M. S. Chance and J. Manickam for

the PEST vacuum comparison, and Dr. S. C. Jardin and J. Delucia for the axisymmetric comparison is greatly appreciated.

This work was supported by United States Department of Energy Contract No. EY-76-C-02-3073.

* Present address: Grumman Aerospace Corporation, 101 College Road East, Princeton, New Jersey 08540.

REFERENCES

1. R. Lust, E. Martenson, Z. Naturforsch, 15a (1960) 706.
2. S. C. Jardin, Phys. Fluids 21, (1978) 1851.
3. R. C. Grimm, J. M. Greene, and J. L. Johnson in Methods in Computational Physics (J. Killeen, Ed.) Vol. 16, Academic Press, New York (1976) 253.
4. R. L. Dewar, Nucl. Fusion 18, (1978) 1541.
5. J. L. Johnson, H. E. Dalhed, J. M. Greene, R. C. Grimm, Y. Y. Hsieh, S. C. Jardin, J. Manickan, M. Okabayashi, R. G. Storer, A. M. M. Todd, D. E. Voss, and K. E. Weimer, J. Comput. Phys. 32, No. 2, (1979) 212.
6. P. M. Morse and H. Feshback, Methods of Theoretical Physics, McGraw Hill (1953) 1302.
7. M. S. Chance, R. L. Dewar, A. M. M. Todd, J. Manickam, R. C. Grimm, J. M. Greene, and J. L. Johnson, Proceedings of the 8th Conference on Numerical Simulation of Plasmas, Monterey (1978).
8. J. H. Malmberg and M. N. Rosenbluth, Rev. Sci. Instrum. 36, (1965) 1886.
9. M. S. Chance, J. M. Greene, R. C. Grimm, and J. L. Johnson Princeton Plasma Physics Laboratory Report MATT 1246 (1976).

TABLE I

METHOD I

M	-2	-1	0	1	2	3	4	5	6
-2	5.401	0.717	-0.862	-0.518	-0.015	0.000	0.000	-0.003	-0.005
-1	0.718	12.868	-0.811	-1.538	-0.209	-0.001	0.027	0.021	0.011
0	-0.868	-0.826	48.343	-0.414	-0.176	-0.001	0.051	0.061	0.055
1	-0.518	-1.538	-0.407	3.240	0.073	0.002	-0.054	-0.039	-0.025
2	-0.015	-0.209	-0.174	0.073	0.221	0.000	-0.025	-0.025	-0.015
3	0.000	-0.001	-0.001	0.002	0.000	0.000	0.000	0.000	0.000
4	0.000	0.027	0.050	-0.054	-0.025	0.000	0.058	0.011	0.027
5	-0.003	0.020	0.058	-0.039	-0.025	0.000	0.011	0.153	0.022
6	-0.005	0.010	0.051	-0.025	-0.015	0.000	0.027	0.022	0.246

METHOD II

M	-2	-1	0	1	2	3	4	5	6
-2	5.402	0.719	-0.862	-0.517	-0.015	0.000	0.000	-0.003	-0.005
-1	0.719	12.872	-0.811	-1.536	-0.209	-0.001	0.027	0.020	0.010
0	-0.862	-0.811	48.341	-0.407	-0.174	-0.001	0.050	0.058	0.051
1	-0.517	-1.536	-0.407	3.241	0.073	0.002	-0.054	-0.039	-0.025
2	-0.015	-0.209	-0.174	0.073	0.221	0.000	-0.025	-0.025	-0.015
3	0.000	-0.001	-0.001	0.002	0.000	0.000	0.000	0.000	0.000
4	0.000	0.027	0.050	-0.054	-0.025	0.000	0.058	0.011	0.027
5	-0.003	0.020	0.058	-0.039	-0.025	0.000	0.011	0.153	0.022
6	-0.005	0.010	0.051	-0.025	-0.015	0.000	0.027	0.022	0.246

Comparison of two methods for calculating the vacuum energy for a toroidal mode number n = 1, poloidal mode numbers m = -2 to 6, with a wall 0.1 minor radii from the plasma. Method I is the version of this paper, and Method II is the current PEST Green's Function version. The plasma equilibrium is dee shaped, with an elongation of 1.65 at an aspect ratio of 3.0

TABLE II

CODE	CASE I	CASE II	CASE III
Time Dependent	0.542	0.542	0.0
PEST	0.565	0.551	0.0

A comparison of δW (PEST) and time dependent calculations for the linear growth rate. Case I is for a wall at infinity. Cases II and III are for the unconnected and connected circuits of Fig. 2a respectively.

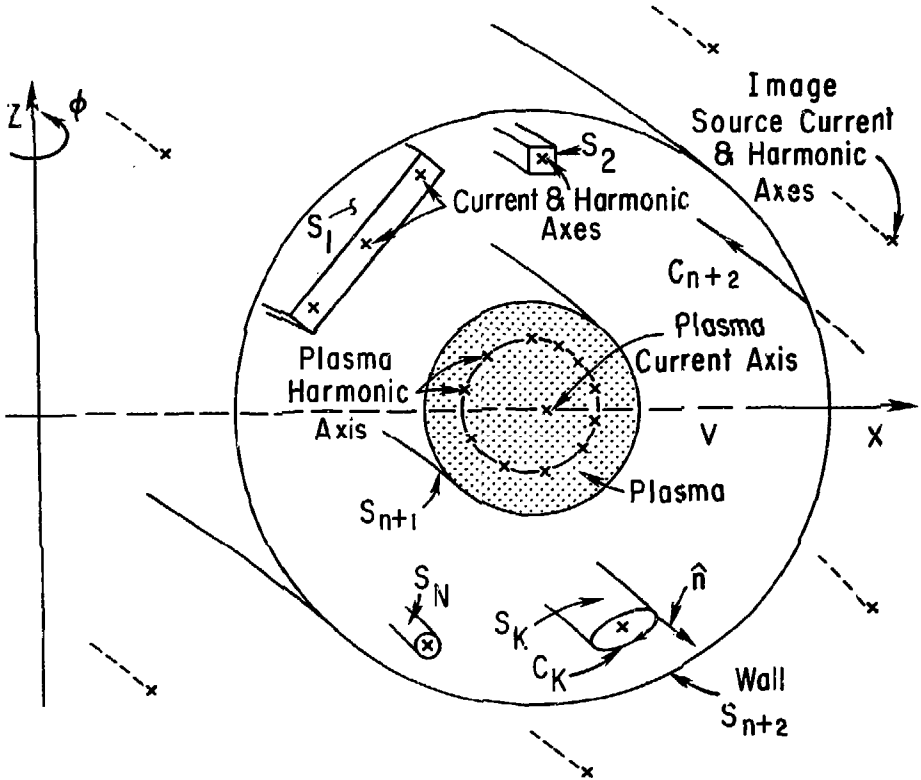

792624

Fig. 1. Schematic diagram of solution domain showing typical conducting elements and source locations.

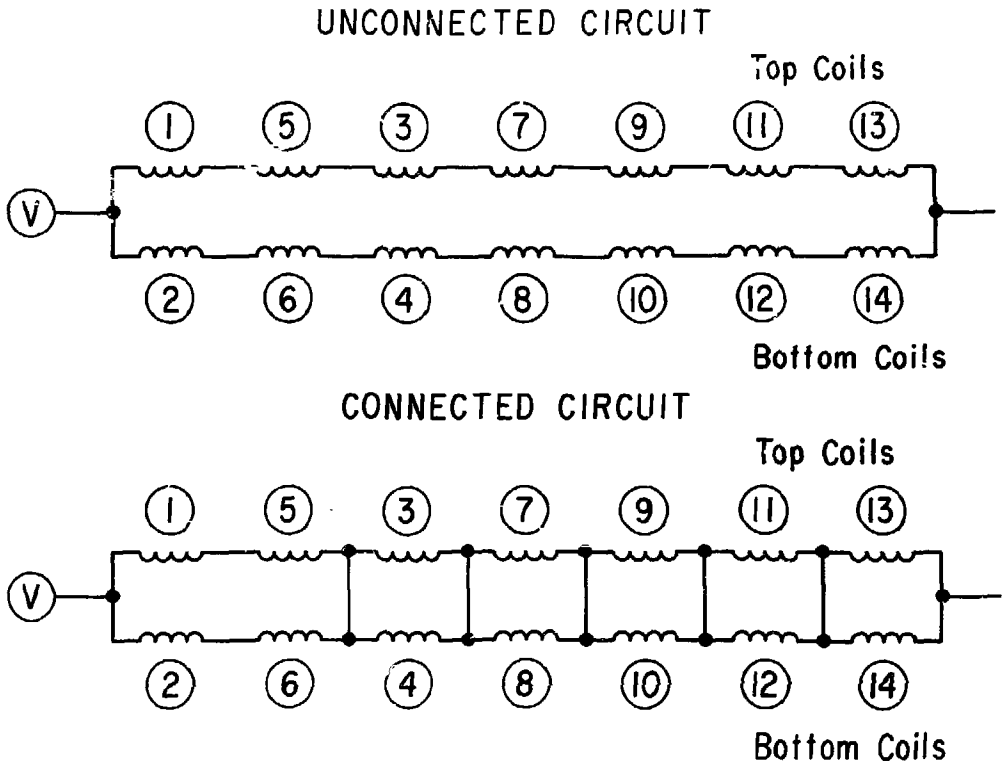

792660

Fig. 2a. PDX external circuit connections considered.

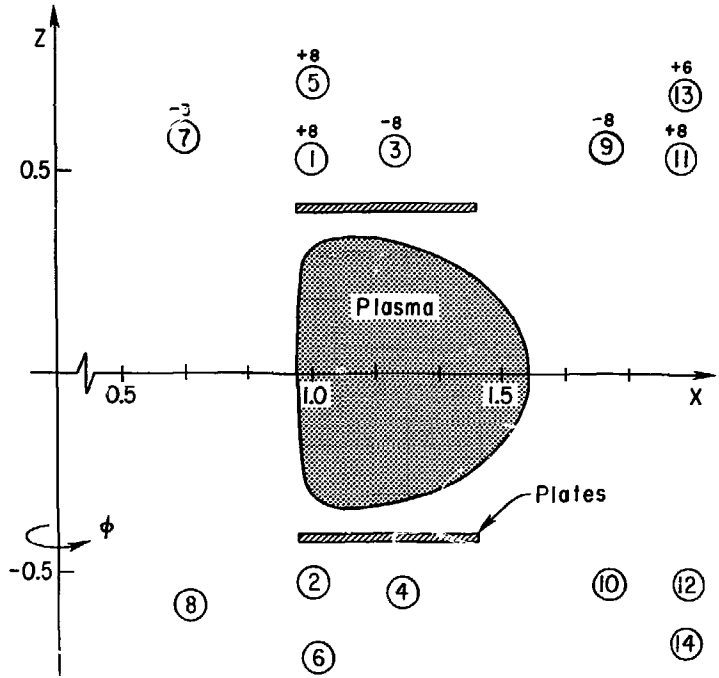

792634

Fig. 2b. Schematic diagram of PDX geometry showing plasma, coil, and plate locations. Turns are noted on the upper coils.